

5. The aromaticity of phosphinine is estimated at 88% of that of benzene [K. K. Baldridge and M. S. Gordon, *J. Am. Chem. Soc.* **110**, 4204 (1988)].
6. F. A. Cotton and G. Wilkinson, in *Advanced Inorganic Chemistry* (Wiley, New York, 1988), pp. 255–259.
7. C. Batich *et al.*, *J. Am. Chem. Soc.* **95**, 929 (1973); J. Waluk, H.-P. Klein, A. J. Ashe III, J. Michl, *Organometallics* **8**, 2804 (1989).
8. Phosphinine gives also stable  $\eta^6$  complexes [C. Eischenbroich *et al.*, *Angew. Chem. Int. Ed. Engl.* **30**, 547 (1991)].
9. C. Eischenbroich *et al.*, *ibid.* **1**, 1343 (1992); C. Eischenbroich *et al.*, *J. Organomet. Chem.* **459**, 157 (1993); C. Eischenbroich *et al.*, *J. Am. Chem. Soc.* **116**, 6217 (1994).
10. P. Le Floch *et al.*, *Inorg. Chem.* **34**, 11 (1995).
11. For a discussion of the conformational problems, see F. Laporte, F. Mercier, L. Ricard, F. Mathey, *J. Am. Chem. Soc.* **116**, 3306 (1994).
12. N. Avarvari, P. Le Floch, F. Mathey, *ibid.* **118**, 11978 (1996); N. Avarvari, P. Le Floch, L. Ricard, F. Mathey, *Organometallics* **16**, 4089 (1997).
13. The  $^{31}\text{P}$  NMR for **3**:  $\delta^{31}\text{P} = 275.9$  [triplet,  $^4J(\text{P-P}) = 12.0$  Hz, phosphinine] and 304.3 [doublet, 1,2-azaphosphinine in toluene];  $\delta$  is the chemical shift, and  $J(\text{P-P})$  is the phosphorus-phosphorus coupling constant.
14. Characterization of **4**:  $\delta^{31}\text{P} = 277.5$  ( $\text{CDCl}_3$ ); mass spectrometry, mass-to charge ( $m/z$ ) ratio (ion, relative intensity): 1216 (M, 12). Elemental analysis calculated for  $\text{C}_{76}\text{H}_{68}\text{P}_4\text{Si}_4$ : C, 75.00; H, 5.59. Found: C, 75.14; H, 5.47.
15. Characterization of **5**:  $\delta^{31}\text{P} = 293.1$  ( $\text{CDCl}_3$ );  $m/z$  (ion, relative intensity): 912 (M, 100). Elemental analysis calculated for  $\text{C}_{57}\text{H}_{51}\text{P}_3\text{Si}_3$ : C, 75.00; H, 5.59. Found: C, 75.12; H, 5.48.
16. Characterization of **6**:  $\delta^{31}\text{P} = 228.2$ ,  $^1J(^{31}\text{P-}^{103}\text{Rh}) = 144.5$  Hz ( $\text{CDCl}_3$ ). Elemental analysis calculated for  $\text{C}_{76}\text{H}_{68}\text{BF}_4\text{P}_4\text{RhSi}_4$ : C, 64.86; H, 4.84. Found: C, 64.69; H, 4.72. Characterization of **7**:  $\delta^{31}\text{P} = 204.8$  ( $\text{CD}_2\text{Cl}_2$ ). Elemental analysis calculated for  $\text{C}_{76}\text{H}_{68}\text{BF}_4\text{P}_4\text{IrSi}_4$ : C, 61.00; H, 4.55. Found: C, 61.17; H, 4.45.
17. B. Breit, R. Winde, K. Harms, *J. Chem. Soc. Chem. Commun.* **1997**, 2681 (1997).
18. Characterization of **8**:  $\delta^{31}\text{P} = 247.0$ ,  $^1J(^{31}\text{P-}^{183}\text{W}) = 236.7$  Hz; MS,  $m/z$  (ion, relative intensity): 1124 ( $\text{M-2xCO}$ , 40). Elemental analysis calculated for  $\text{C}_{60}\text{H}_{51}\text{O}_3\text{P}_3\text{Si}_3\text{W}$ : C, 61.02; H, 4.32. Found: C, 61.15; H, 4.25.
19. P. Le Floch, L. Ricard, F. Mathey, *Polyhedron* **9**, 991 (1990).
20. F. A. Walker and U. Simonis, *Encyclopedia of Inorganic Chemistry*, R. B. King, Ed. (Wiley, Chichester, UK, 1994), pp. 1785–1846.
21. A. Sorokin, J. L. Séris, B. Meunier, *Science* **268**, 1163 (1995).
22. We thank the CNRS and Ecole Polytechnique for financial support.

23 February 1998; accepted 23 April 1998

## High- $T_c$ Superconductors in the Two-Dimensional Limit: $[(\text{Py-C}_n\text{H}_{2n+1})_2\text{HgI}_4]\cdot\text{Bi}_2\text{Sr}_2\text{Ca}_{m-1}\text{Cu}_m\text{O}_y$ ( $m = 1$ and $2$ )

Jin-Ho Choy,\* Soon-Jae Kwon, Gyeong-Su Park

The free modulation of interlayer distance in a layered high-transition temperature (high- $T_c$ ) superconductor is of crucial importance not only for the study of the superconducting mechanism but also for the practical application of high- $T_c$  superconducting materials. Two-dimensional (2D) superconductors were achieved by intercalating a long-chain organic compound into bismuth-based high- $T_c$  cuprates. Although the intercalation of the organic chain increased the interlayer distance remarkably, to tens of angstroms, the superconducting transition temperature of the intercalate was nearly the same as that of the pristine material, suggesting the 2D nature of the high- $T_c$  superconductivity.

Since the appearance of layered cuprate superconductors, much attention has been given to elucidating the origin of high- $T_c$  superconductivity, such as the interlayer coupling effect (1–3), in-plane charge carrier density (4–6), or both. According to the model of Wheatley, Hsu, and Anderson, the superconducting transition temperature  $T_c$  of a layered cuprate superconductor is expressed as

$$T_c = \lambda_0 + \lambda_1 \quad (1)$$

where  $\lambda_0$  is the interlayer coupling between the nearest  $\text{CuO}_2$  planes (intra-block coupling) and  $\lambda_1$  is the interlayer coupling between the next nearest planes (interblock coupling) (1). However, Uemura *et al.* have suggested a close correlation between  $T_c$  and 2D carrier density ( $n_s/m^*$ , where  $n_s$  is the superconducting carrier density and  $m^*$  is the effective mass) in the layered high- $T_c$  superconductor (4). The issues are still controversial. To solve such problems, a way to freely modulate the interlayer distance without perturbing the superconducting oxide block is needed. Here, we developed model compounds where organic modulation layers are intercalated into  $\text{Bi}_2\text{O}_2$  double layers of the high- $T_c$  cuprate superconductors,  $\text{Bi}_2\text{Sr}_2\text{Ca}_{m-1}\text{Cu}_m\text{O}_y$  ( $m = 1$  and  $2$ ; Bi2201 and Bi2212). In such intercalates,

the interlayer distance of the superconductive  $\text{CuO}_2$  layer can be easily controlled by changing the number of carbon atoms in the organic chain. The present organic intercalates with remarkable layer separation can be regarded as 2D limit cuprate superconductors, taking into account the small out-of-plane coherence length ( $\xi_c$ ) in the pristine materials (7). The magnetization studies on the intercalates reveal that the high- $T_c$  superconductivity is retained even in the nearly isolated  $\text{CuO}_2$  plane. The organic intercalates are also regarded as weakly coupled Josephson multilayers, where the barrier width greatly influences the diamagnetic shielding fraction. In this respect, the present organic-inorganic hybrids can be an ideal model compound to investigate low-dimensional superconducting theories such as the Kosterlitz-Thouless transition (8) and the Lawrence-Doniach model (9) in high- $T_c$  materials. Moreover, the intercalation of long-chain organic molecules can minimize the interaction between the cuprate building blocks, leading to an isolated single sheet by exfoliation. The superconducting nanoparticle, obtained in such a way, can be a precursor for the fabrication of ultrathin superconducting films.

We intercalated long-chain organic compounds into Bi-based high- $T_c$  cuprates in the form of the complex salt bisalkylpyridinium tetraiodomercurate  $[(\text{Py-C}_n\text{H}_{2n+1})_2\text{HgI}_4]$ . The x-ray diffraction (XRD) analyses and the high-resolution electron microscope (HREM) images of these intercalates show that the organic spacer layers with various thicknesses are stabilized in between the  $\text{Bi}_2\text{O}_2$  double layers of Bi-based high- $T_c$  cuprates.

The Bi-based cuprate superconductors have weakly bound  $\text{Bi}_2\text{O}_2$  double layers that make it possible to intercalate various guest species without introducing any substantial changes to the superconducting block (10–14). The pristine  $\text{Bi}_2\text{Sr}_2\text{Ca}_{m-1}\text{Cu}_m\text{O}_y$  ( $m = 1$  and  $2$ ) compounds (15) were synthesized by conventional solid state reaction with the nominal compositions of  $\text{Bi}_2\text{Sr}_{1.6}\text{La}_{0.4}\text{CuO}_x$  (Bi2201) for  $m = 1$  and  $\text{Bi}_2\text{Sr}_{1.5}\text{Ca}_{1.5}\text{Cu}_2\text{O}_y$  (Bi2212) for  $m = 2$ , where the Sr ion is partially substituted by the La ion or Ca ion to obtain single-phase samples. The intercalation of an organic chain into the pristine material was achieved with the following stepwise synthesis. First, the  $\text{HgI}_2$ -intercalated  $\text{Bi}_2\text{Sr}_2\text{Ca}_{m-1}\text{Cu}_m\text{O}_y$  ( $m = 1$  and  $2$ ;  $\text{HgI}_2$ -Bi2201 and  $\text{HgI}_2$ -Bi2212) compounds were prepared by heating the guest  $\text{HgI}_2$  and the pristine materials in a vacuum-sealed Pyrex tube, as reported previously (13). Then, the intercalation of the organic chain was car-

Jin-Ho Choy and Soon-Jae Kwon, Department of Chemistry, Center for Molecular Catalysis, College of Natural Sciences, Seoul National University, Seoul 151-742, Korea.

Gyeong-Su Park, Samsung Advanced Institute of Technology, Post Office Box 111, Suwon 440-660, Korea.

\*To whom correspondence should be addressed. E-mail: jhchoy@plaza.snu.ac.kr

ried out by the solvent-mediated reaction between  $\text{HgI}_2$  intercalates and alkylpyridinium iodide. The reactants of  $\text{Py-C}_n\text{H}_{2n+1}\text{I}$  ( $n = 1, 2, 4, 6, 8, 10, \text{ and } 12$ ) were obtained by reacting alkyl iodide with 1 M equivalent of pyridine in diethyl-ether solvent. The  $\text{HgI}_2$  intercalates were mixed with two excess reactants of  $\text{Py-C}_n\text{H}_{2n+1}\text{I}$ , to which a small amount of dried acetone (0.5 ml per 1 g of the mixture) was added. Each solvent-containing mixture was reacted in a closed ampoule at  $40^\circ\text{C}$  for 6 hours

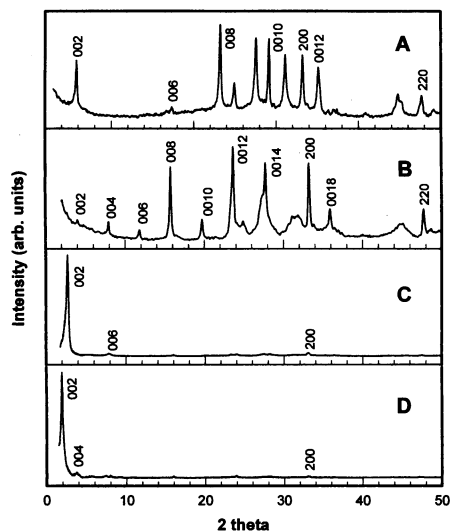


**Fig. 1.** Powder XRD patterns for (A) pristine  $\text{Bi2212}$ , (B)  $\text{HgI}_2$ - $\text{Bi2212}$ , and (C and D) the  $(\text{Py-C}_n\text{H}_{2n+1})_2\text{HgI}_4$ - $\text{Bi2212}$  series with  $n = 6$  (C) and  $n = 12$  (D), respectively. arb. units, arbitrary units.

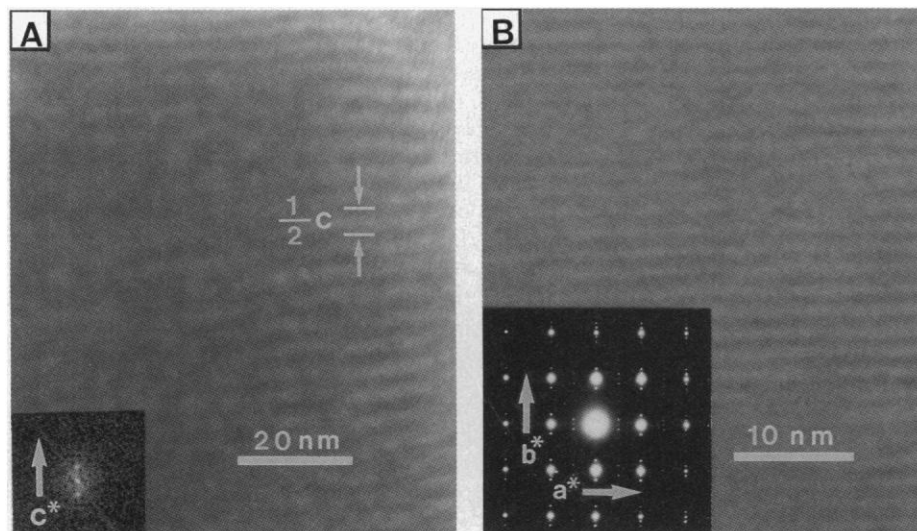


**Fig. 2.** (A) An HREM image of the thin cross section of a  $(\text{Py-C}_n\text{H}_{2n+1})_2\text{HgI}_4$ - $\text{Bi2212}$  ( $n = 12$ ) particle and (inset) its Fourier diffractogram revealing periodic arrangement of the layered nanocomposite. The basal spacing ( $1/2c \approx 47 \text{ \AA}$ ) is consistent with the XRD and  $c^*$  represents  $[001]_{\text{Bi2212}}$  orientation. The HREM image was obtained with H-9000NA equipment at an accelerating voltage of 300 kV. (B) A high-resolution plane view of the organic intercalate ( $n = 12$ ) and (inset) its electron diffraction pattern, where the organic material  $(\text{Py-C}_n\text{H}_{2n+1})_2\text{HgI}_4$  on the surface of the sectioned plane was cleaned with chloroform.

and washed with a solvent blend of acetone and diethyl-ether (1:1 volumetric ratio) to remove the excess reactant of  $\text{Py-C}_n\text{H}_{2n+1}\text{I}$ . The resulting products were dried in vacuum. The samples are all air-stable.

The formation of single-phase stage 1 intercalates was confirmed by powder XRD analyses and also by cross-sectional view of HREM images. According to electron probe microanalysis and elemental analyses for C, H, and N, the chemical formulas of organic intercalates were determined to be  $[(\text{Py-C}_n\text{H}_{2n+1})_2\text{HgI}_4]_{0.35}\text{Bi}_2\text{Sr}_{1.6}\text{La}_{0.4}\text{CuO}_x$ ,  $[(\text{Py-C}_n\text{H}_{2n+1})_2\text{HgI}_4\text{-Bi2201}]$  and  $[(\text{Py-C}_n\text{H}_{2n+1})_2\text{HgI}_4]_{0.35}\text{Bi}_2\text{Sr}_{1.5}\text{Ca}_{1.5}\text{Cu}_2\text{O}_y$ ,  $[(\text{Py-C}_n\text{H}_{2n+1})_2\text{HgI}_4\text{-Bi2212}]$ , which are identical to the nominal compositions within the limit of experimental error, indicating that the inorganic host lattice is not chemically modified after the intercalation. The effect of intercalation on superconductivity was examined by a dc superconducting quantum interference device (SQUID) magnetometer.

The powder XRD patterns for the pristine  $\text{Bi2212}$ ,  $\text{HgI}_2$  intercalate, and  $(\text{Py-C}_n\text{H}_{2n+1})_2\text{HgI}_4$  intercalates ( $n = 6$  and  $12$ ) are shown in Fig. 1. There is no trace of the pristine phase in the XRD patterns of all of the present intercalates, indicating that  $\text{HgI}_2$  and organic complexes are intercalated homogeneously into the host lattice. According to the least squares fitting analysis, each intercalated organic spacer layer expands the unit cell along the  $c$  axis by 10.8, 11.3, 13.7, 17.7, 22.9, 26.7, and 31.6 for  $n = 1, 2, 4, 6, 8, 10, \text{ and } 12$ , respectively.

An HREM image with a Fourier diffractogram of the cross section of an organic-inorganic nanocomposite particle obtained by ultramicrotomy is shown in Fig. 2A. It appears to feature well-aligned planes with detailed texture in the form of discrete bright lines, illustrating the presence of organic bilayers. Moreover, the high-resolution plane view of the organic intercalate ( $n = 12$ ) and its electron diffraction pattern illustrating atomic arrangement of the  $[100]_{\text{Bi2212}}$  and  $[010]_{\text{Bi2212}}$  orientations show that the cuprate lattice is not perturbed upon organic intercalation (Fig. 2B). The relation between the hydrocarbon chain length and the interlayer distance  $d$  in the organic intercalates, where  $d$  is linearly proportional to the number of aliphatic carbon atoms ( $n$ ) in the range  $n = 4$  to  $12$  of  $\text{Py-C}_n\text{H}_{2n+1}$ , is shown in Fig. 3A. On the basis of the calculated slope of  $\Delta d/n = 2.42 \text{ \AA}$ , it is suggested that the bilayered alkyl chains are stabilized in between  $\text{Bi}_2\text{O}_2$  layers with a tilting angle of  $70^\circ$  with respect to the basal plane (Fig. 3, B and C).

To understand the effect of intercala-

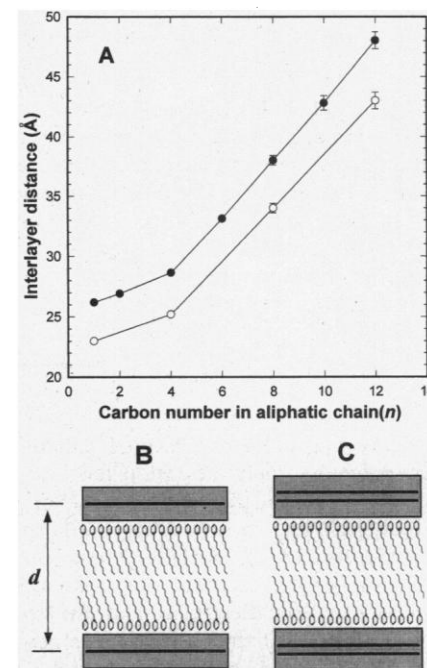


**Fig. 3.** (A) Interlayer distance ( $d$ ) as a function of the number of carbon atoms in aliphatic chains of the intercalant for  $(\text{Py-C}_n\text{H}_{2n+1})_2\text{HgI}_4$ - $\text{Bi2201}$  ( $\circ$ ) and  $(\text{Py-C}_n\text{H}_{2n+1})_2\text{HgI}_4$ - $\text{Bi2212}$  ( $\bullet$ ). As the aliphatic chain length increases ( $n \geq 4$ ), the basal increment becomes larger because of the Van der Waals energy gain between organic chains. (B and C) Schematic illustrations of the decylpyridinium ( $n = 10$ ) derivative of  $\text{Bi2201}$  intercalate (B) and that of the  $\text{Bi2212}$  intercalate (C), where the anions ( $\text{HgI}_4^{2-}$ ) are sandwiched in between the pyridinium cations but omitted here for simplicity.

tion on the electronic structure of the superconducting CuO<sub>2</sub> layer, we measured the Cu K edge x-ray absorption near-edge structure (XANES) spectra for the pristine Bi2212 and its intercalates. Figure 4, A and B, represents the Cu K edge XANES spline and the second derivative spectra for Bi2212 and (Py-C<sub>n</sub>H<sub>2n+1</sub>)<sub>2</sub>HgI<sub>4</sub>-Bi2212 (*n* = 1 and 12), respectively, together with those for some references. As shown in Fig. 4, the organic intercalates exhibit the characteristic peaks of the Bi-based cuprate corresponding to the dipole-allowed transitions from core 1s level to unoccupied 4p states, which are denoted as A, A', B, and C, together with the pre-edge peak P corresponding to the quadrupole-allowed transition of 1s → 3d. Among these states, the position and in-

tensity of peak A have been known to reflect sensitively the local structure around copper (16). On the other hand, according to the Bi L<sub>III</sub> edge XANES study, the overall spectral features of the organic intercalates are similar to those of the pristine material.

The local structure of Hg in the intercalated layer was investigated by performing the Hg L<sub>III</sub> edge extended x-ray absorption fine-structure analysis for the organic intercalates and the reference (Py-C<sub>n</sub>H<sub>2n+1</sub>)<sub>2</sub>HgI<sub>4</sub>. Although the intercalated HgI<sub>2</sub> in HgI<sub>2</sub>-Bi2212 has been revealed to have a two-coordinate linear structure (13, 14), the present results indicate that the Hg species of the organic intercalates is stabilized as a HgI<sub>4</sub><sup>2-</sup> tetrahedron (17, 18), confirming the formation of complex salt between Py-C<sub>n</sub>H<sub>2n+1</sub>I and HgI<sub>2</sub> in the Bi<sub>2</sub>O<sub>2</sub> interlayer space. In this respect, the intercalation mechanism for the complex salt is suggested to be quite different from that for iodine (10–12) and mercuric halides (13, 14), where a small fraction of electronic charge is transferred from the cuprate block to the intercalant layer. In the present organic intercalates, the major driving force of intercalation is considered to be a negative enthalpy change ( $\Delta H$ ) during the formation of a tetraiodomercurate complex anion (HgI<sub>4</sub><sup>2-</sup>): For HgI<sub>2</sub> + 2I<sup>-</sup> → HgI<sub>4</sub><sup>2-</sup>,  $\Delta H = -95.8$  kJ/mol (19), and, in the course of this reaction, the organic cation is also inserted into the Bi<sub>2</sub>O<sub>2</sub> layer to meet the condition of charge neutrality. Considering the ionic character of the guest species, it is suggested that there is a partial distortion of local charge (local charge separation) in the Bi–O charge reservoir plane, giving rise to

a weak electrostatic attraction between guest and host.

The zero-field-cooled (ZFC) dc magnetizations of the pristine Bi2212 and its intercalates were measured as a function of temperature (Fig. 5A). In spite of a remarkable expansion of basal spacing, all of the organic intercalates exhibit superconductivity with an onset *T*<sub>c</sub> of 81 to 82 K, which is higher than those for the iodine intercalate (10–12) (*T*<sub>c</sub> ≈ 63 K,  $\Delta d \approx 3.6$ ) and the HgI<sub>2</sub> intercalate (*T*<sub>c</sub> ≈ 68 K,  $\Delta d \approx 7.2$ ) and even slightly greater than that for the pristine material (*T*<sub>c</sub> ≈ 78 K). Because the organic intercalates are made by the reaction between the HgI<sub>2</sub> intercalate and alkyipyridinium iodide, there should be, if any, the same amount of unintercalated remnant of the pristine Bi2212 in both type of intercalates, resulting in similar magnetic behavior near the transition temperature (78 K) of the pristine material. However, HgI<sub>2</sub>-Bi2212 and (Py-C<sub>n</sub>H<sub>2n+1</sub>)<sub>2</sub>HgI<sub>4</sub>-Bi2212 exhibit different magnetic behavior at around 78 K (Fig. 5A). Furthermore, the organic intercalates show higher onset *T*<sub>c</sub> values compared with the HgI<sub>2</sub> intercalate. Figure 5B shows the relation between *T*<sub>c</sub> and the separation between the CuO<sub>2</sub> planes in adjacent blocks, where the *T*<sub>c</sub> values of the intercalates are insensitive to the interlayer distance but are mainly dependent on the nature of the intercalant. Such findings are very interesting in light of the interlayer coupling theory in high-*T*<sub>c</sub> superconductivity, which predicts that *T*<sub>c</sub> is proportional to the coupling strength between adjacent superconducting layers, that is, inversely proportional to the layer separation [*k*<sub>B</sub>*T*<sub>c</sub> ∝ (ε*d*)<sup>-1</sup>, where *k*<sub>B</sub> is the

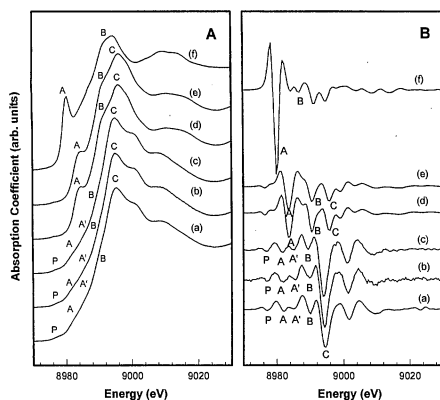


**Fig. 4.** (A) Cu K edge XANES spline and (B) second derivative spectra for (a) the pristine Bi2212, (b) and (c) the organic intercalates (Py-C<sub>n</sub>H<sub>2n+1</sub>)<sub>2</sub>HgI<sub>4</sub>-Bi2212 with *n* = 1 (b) and *n* = 12 (c), and other reference compounds [Cu<sub>2</sub>O (d), CuO (e), and Cu(OH)<sub>2</sub> (f)].

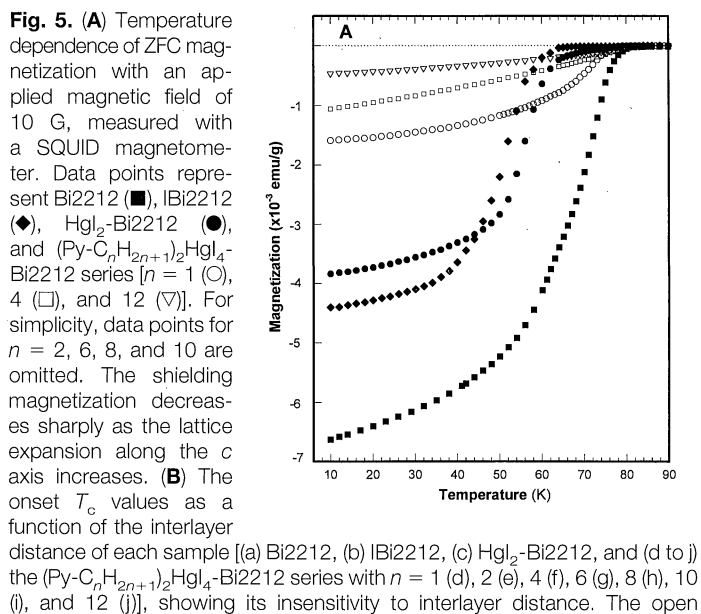
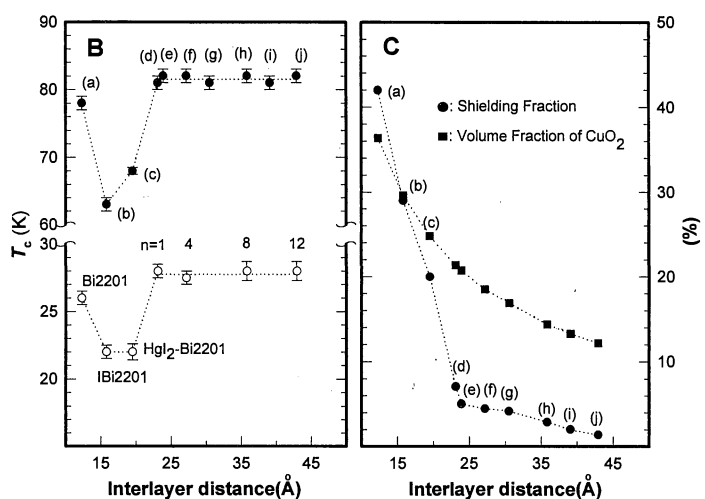


**Fig. 5.** (A) Temperature dependence of ZFC magnetization with an applied magnetic field of 10 G, measured with a SQUID magnetometer. Data points represent Bi2212 (■), lBi2212 (●), HgI<sub>2</sub>-Bi2212 (◆), and (Py-C<sub>n</sub>H<sub>2n+1</sub>)<sub>2</sub>HgI<sub>4</sub>-Bi2212 series [*n* = 1 (○), 4 (□), and 12 (▽)]. For simplicity, data points for *n* = 2, 6, 8, and 10 are omitted. The shielding magnetization decreases sharply as the lattice expansion along the *c* axis increases. (B) The onset *T*<sub>c</sub> values as a function of the interlayer distance of each sample [(a) Bi2212, (b) lBi2212, (c) HgI<sub>2</sub>-Bi2212, and (d) to (j) the (Py-C<sub>n</sub>H<sub>2n+1</sub>)<sub>2</sub>HgI<sub>4</sub>-Bi2212 series with *n* = 1 (d), 2 (e), 4 (f), 6 (g), 8 (h), 10 (i), and 12 (j)], showing its insensitivity to interlayer distance. The open



circles represent the Bi2201 series. (C) The diamagnetic shielding fraction and calculated volume ratio of the CuO<sub>2</sub> bilayer for the Bi2212 series as a function of interlayer distance. Samples correspond to (B).

Boltzmann constant and  $\epsilon$  is the dielectric constant] (2). The broadness of the superconducting transition observed for the organic intercalates (Fig. 5A) is attributed to the thermal fluctuation in the true 2D superconductor (20).

The depressed  $T_c$  value upon  $\text{HgI}_2$  intercalation is recovered by the intercalation of organic salt, which can be understood as a result of charge restoration of the host block. Because of the ionic-bonding character of the guest species  $(\text{Py-C}_n\text{H}_{2n+1})_2\text{HgI}_4$  itself, a charge transfer between host block and intercalant layer would not be expected (21), in contrast to the halogen or mercuric halide intercalates (10–14).

To investigate the evolution of superconductivity in a single-layer superconductor, we also measured magnetizations for the organic intercalates of  $(\text{Py-C}_n\text{H}_{2n+1})_2\text{HgI}_4\text{-Bi2201}$ , where the basal increment ( $\Delta d$ ) corresponds to 10.9, 13.1, 22.4, and 31.9 Å for  $n = 1, 4, 8,$  and 12, respectively. The superconductivity of Bi2201 is also retained upon intercalation of a long-chain organic compound. Moreover, although  $T_c$  is depressed ( $\Delta T_c \approx 4$  K) upon iodine and  $\text{HgI}_2$  intercalation, all of the organic intercalates of Bi2201 show superconductivity with onset  $T_c$  values of 27 to 28 K, comparable to that of the pristine Bi2201 ( $T_c \approx 26$  K) (Fig. 5B). Such results allow us to conclude that  $T_c$  in the layered cuprate is essentially governed by the intrinsic property of a single  $\text{CuO}_2$  plane rather than by the interlayer electronic coupling effect. Because there is only one  $\text{CuO}_2$  plane per cuprate building block, the long-organic-chain-intercalated Bi2201 is believed to be a genuine single-layer superconductor because of the large interlayer distance compared with the  $c$ -axis coherence length of layered cuprates ( $d \gg \xi_c$ ). On the basis of these findings, it becomes clear that a 2D single cuprate sheet in the organic intercalate exhibits high- $T_c$  superconductivity.

The superconducting shielding fractions of the pristine Bi2212 and its intercalates are represented in Fig. 5C as a function of distance ( $d$ ) between interblock  $\text{CuO}_2$  planes, where the shielding fraction decreases drastically as  $d$  increases. A modification of interlayer distance has a more substantial effect on the diamagnetic shielding fraction than on the volume fraction of the  $\text{CuO}_2$  layer. The present superconducting compounds interstratified with organic spacer layers can be regarded as weakly coupled Josephson multilayers, because their structures are periodic sequences with a fashion of superconducting-insulating-superconducting. In the present setup of magnetic prop-

erty measurement, all of the grains in polycrystalline samples are randomly oriented with respect to the applied magnetic field. In this respect, such a decrease of shielding fraction with increasing  $d$  can be explained by the exponentially decreasing Josephson tunneling rate with increasing insulating barrier (22). This explanation is supported by our previous magnetization study on the grain-aligned  $\text{HgI}_2\text{-Bi2212}$  (23), where the shielding fractions of the aligned samples at 10 K are 67% for the pristine Bi2212 ( $d \approx 12$  Å) and 61% for  $\text{HgI}_2\text{-Bi2212}$  ( $d \approx 20$  Å) whereas those of nonaligned samples are  $\sim 42\%$  for the former and  $\sim 21\%$  for the latter. The difference between the aligned sample and the nonaligned one is attributed to the contribution of  $c$ -axis tunneling, because the superconducting planes are perpendicular (in-plane supercurrent) to the applied field in the former, whereas they are randomly oriented (both in-plane and Josephson supercurrent) in the latter. Such results allow us to conclude that the increasing barrier thickness is mainly responsible for the drastic decrease of diamagnetic shielding fraction in the intercalated system.

Until now, the interlayer coupling effects and low-dimensional properties of high- $T_c$  superconductors have been investigated by the sequential deposition of alternating layers of a superconducting YBCO layer and an insulating PrBCO layer in vacuum (3, 24). In such a YBCO-PrBCO superlattice compound, however, there exist other factors affecting  $T_c$ , such as strain effect by lattice mismatching, interdiffusion of Y and Pr atoms, proximity effect, and hole doping between sublattices, in addition to a change in the interlayer distance. The present organic intercalate has no substantial stress on the superconducting layer because of the weak interaction between host and guest. Furthermore, the hydrocarbon chain in the intercalant layer is a true insulator. In this regard, these intercalates have provided a clue that high- $T_c$  superconductivity of layered cuprate is an intrinsic 2D nature as in the case of low- $T_c$  TaS<sub>2</sub>-amine compounds (25). And the cuprate layers separated by an organic barrier are surely believed to be molecular-level thin films of a high- $T_c$  superconductor, which are most suitable for studying the weakly coupled or decoupled vortex behavior (26) in the type II superconductor because of their freely modifiable interlayer distance. In addition, the present multilayered superconductors are anticipated to be ideal model systems for understanding the  $c$ -axis properties of layered superconductors (27) in relation to the still controversial issues in

the high- $T_c$  mechanism. It is now expected that the newly synthesized organic cuprate hybrids will provide substantial data for testing various existing theories explaining the 2D superconductivity.

From the viewpoint of applications, the intercalation of a large molecule into a layered superconductor can be a new route to the nanoengineering of a high- $T_c$  superconductor, because it can offer a method for separating the layered superconductor into isolated single sheets. Moreover, the synthetic technique developed through this work is expected to be quite useful in the synthesis of many other new intercalation compounds.

## REFERENCES AND NOTES

1. J. M. Wheatly, T. C. Hsu, P. W. Anderson, *Nature* **333**, 121 (1988).
2. D. R. Harshman and A. P. Mills, *Phys. Rev. B* **45**, 10684 (1992).
3. Q. Li *et al.*, *Phys. Rev. Lett.* **64**, 3086 (1990).
4. Y. J. Uemura *et al.*, *ibid.* **62**, 2317 (1989).
5. J. Ihm and B. D. Yu, *Phys. Rev. B* **39**, 4760 (1989).
6. M. Di Stasio, K. A. Müller, L. Pietronero, *Phys. Rev. Lett.* **64**, 2827 (1990).
7. R. Kleiner and P. Müller, *Phys. Rev. B* **49**, 1327 (1994).
8. J. M. Kosterlitz and D. J. Thouless, *J. Phys. C* **6**, 1181 (1973).
9. W. E. Lawrence and S. Doniach, in *Proceedings of the 12th International Conference on Low-Temperature Physics*, E. Kanda, Ed. (Academic Press, Kyoto, Japan, 1971), pp. 361–362.
10. X.-D. Xiang *et al.*, *Nature* **348**, 145 (1990).
11. X.-D. Xiang *et al.*, *Phys. Rev. B* **43**, 11496 (1991).
12. G. Liang *et al.*, *ibid.* **47**, 1029 (1993).
13. J. H. Choy, N. G. Park, S. J. Hwang, D. H. Kim, N. H. Hur, *J. Am. Chem. Soc.* **116**, 11564 (1994).
14. J. H. Choy, S. J. Hwang, N. G. Park, *ibid.* **119**, 1624 (1997).
15. H. Maeda, T. Tanaka, M. Fukutomi, T. Asano, *Jpn. J. Appl. Phys.* **27**, L209 (1987).
16. J. H. Choy, D. K. Kim, S. H. Hwang, G. Demazeau, *Phys. Rev. B* **50**, 16631 (1994).
17. M. Körfer, H. Fuess, J. W. Bats, *Z. Anorg. Allg. Chem.* **354**, 104 (1986).
18. R. H. Fenn, *Acta Crystallogr.* **20**, 24 (1966).
19. R. Arnek and D. Poceva, *Acta Chem. Scand. Ser. A* **30**, 59 (1976).
20. P. A. Bancel and K. E. Gray, *Phys. Rev. Lett.* **46**, 148 (1981).
21. H. Selig and L. B. Ebert, *Adv. Inorg. Chem. Radiochem.* **23**, 281 (1980).
22. J. R. Clem and M. W. Coffey, *Phys. Rev. B* **42**, 6209 (1991).
23. M. K. Bae *et al.*, *ibid.* **53**, 12416 (1996).
24. J. M. Triscone *et al.*, *Phys. Rev. Lett.* **64**, 804 (1990); D. P. Norton, D. H. Lowndes, S. J. Pennycook, J. D. Budai, *ibid.* **67**, 1358 (1991); T. Terashima *et al.*, *ibid.*, p. 1362.
25. F. R. Gamble *et al.*, *Science* **174**, 493 (1971).
26. D. R. Nelson, *Nature* **375**, 356 (1995); E. Zeldov, *ibid.*, p. 373; S. W. Pierson, *Phys. Rev. Lett.* **75**, 4674 (1995).
27. A. J. Leggett, *Science* **274**, 587 (1996); K. A. Moler, J. R. Kirtley, D. G. Hinks, T. W. Li, M. Xu, *ibid.* **279**, 1193 (1998); P. W. Anderson, *ibid.*, p. 1196.
28. Supported in part by the Ministry of Science and Technology for the high- $T_c$  research, by the Korean Science and Engineering Foundation through the Center of Excellency, and by the Basic Science Research Institute Program, Ministry of Education (BSRI-97-3413).

24 February 1998; accepted 14 April 1998